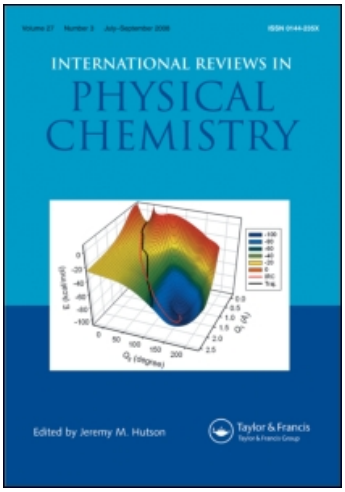

International Reviews in Physical Chemistry
Publication details, including instructions for authors and subscription information:
http://www.informaworld.com/smpp/title~content=t713724383

Investigating the phase-dependent photochemical reaction dynamics of chlorine dioxide using resonance Raman spectroscopy

Sophia C. Hayes; Paul M. Wallace; Josh C. Bolinger; Philip J. Reid

Online publication date: 26 November 2010

To cite this Article Hayes, Sophia C. , Wallace, Paul M. , Bolinger, Josh C. and Reid, Philip J.(2002) 'Investigating the phase-dependent photochemical reaction dynamics of chlorine dioxide using resonance Raman spectroscopy', International Reviews in Physical Chemistry, 21: 3, 405 — 432
To link to this Article: DOI: 10.1080/01442350210156024
URL: http://dx.doi.org/10.1080/01442350210156024

INT. REVIEWS IN PHYSICAL CHEMISTRY, 2002
VOL. 21, NO. 3, 405–432

Taylor & Francis
Taylor & Francis Group

Investigating the phase-dependent photochemical reaction dynamics of chlorine dioxide using resonance Raman spectroscopy

SOPHIA C. HAYES, PAUL M. WALLACE, JOSH C. BOLINGER and PHILIP J. REID†

Box 351700, Department of Chemistry, University of Washington, Seattle, WA 98195, USA

Recent progress in understanding the phase-dependent reactivity demonstrated by halooxides is outlined. Specifically, resonance Raman intensity analysis (RRIA) and time-resolved resonance Raman (TRRR) studies of chlorine dioxide (OClO) photochemistry in solution are presented. Using RRIA, it has been determined that the excited-state structural evolution that occurs along the asymmetric-stretch coordinate in the gas phase is restricted in solution. The absence of evolution along this coordinate results in the preservation of ground-state symmetry in the excited state. The role of symmetry in defining the reaction coordinate and the solvent–solute interactions responsible for modification of the excited-state potential energy surface are discussed. TRRR studies are presented which demonstrate that geminate recombination of the primary photoproducts resulting in the reformation of ground-state OClO is a central feature of OClO photochemistry in solution. These studies also demonstrate that a fraction of photoexcited OClO undergoes photoisomerization to form ClOO, with the ground-state thermal decomposition of this species resulting in Cl production on the subnanosecond timescale. Finally, time-resolved anti-Stokes experiments are presented which demonstrate that the OClO vibrational-relaxation dynamics are solvent dependent. The current picture of OClO photochemistry derived from these studies is discussed, and future directions for study are outlined.

Contents

PAGE

1. Introduction 406

2. The excited-state reaction dynamics of OClO 407
2.1. Background 407
2.2. RRIA of OClO in the gas and condensed phases 409
2.3. The role of symmetry in OClO photochemistry 411
2.4. Solvent response to OClO photoexcitation 413

3. OClO photoproduct formation dynamics 416
3.1. Background 416
3.2. Geminate recombination of the OClO primary photoproducts 417
3.3. The vibrational relaxation dynamics and OClO 421
3.4. Theoretical models for vibrational relaxation in OClO 423
3.5. The production of Cl 425

†Author to whom correspondence should be addressed. Email: preid@chem.washington.edu

International Reviews in Physical Chemistry ISSN 0144–235X print/ISSN 1366–591X online © 2002 Taylor & Francis Ltd
http://www.tandf.co.uk/journals
DOI: 10.1080/01442350210156024

4. Current picture of aqueous OClO photochemistry 428

Acknowledgements 429

References 430

1. Introduction

The hypothesis that anthropogenic compounds were responsible for the transport and production of atomic chlorine in the stratosphere provided the impetus for studies of the halogen-based chemistry that results in stratospheric ozone loss [1–4]. From this work, numerous chemical and photochemical processes have been identified as important in the uptake and release of atomic chlorine (Cl), a central species responsible for ozone depletion [5, 6]. Furthermore, these studies have shown that the chemistry in both homogeneous and heterogeneous environments is of importance. The construction of stratospheric chemical models requires accurate knowledge of the rates and product-formation quantum yields for these processes and how these parameters vary as a function of environment [4, 7, 8]. For example, aerosols or polar stratospheric clouds can promote chemistry that is significantly different from that which occurs in the gas phase. The current challenge in this area is to determine the extent to which a given reaction changes as a function of environment and to understand the fundamental reasons behind this behaviour.

We have been particularly interested in the photochemistry of halooxides such as chlorine dioxide (OClO) [9–13]. This compound is of interest owing to its participation in many stratospheric photochemical processes, and for its role as an indicator of stratospheric chlorine activation [14, 15]. The following reaction channels are available to OClO following photoexcitation [11]:

$$\mathrm{OClO}(\mathrm{X}^2\mathrm{B}_2) \xrightarrow{h\nu} \mathrm{ClO}(^2\Pi) + \mathrm{O}(^3\mathrm{P}_g), \tag{1}$$

$$\mathrm{OClO}(\mathrm{X}^2\mathrm{B}_2) \xrightarrow{h\nu} \mathrm{Cl}(^2\mathrm{P}_u) + \mathrm{O}_2(^1\Delta_g, {}^3\Sigma_g^-), \tag{2}$$

$$\mathrm{OClO}(\mathrm{X}^2\mathrm{B}_2) \xrightarrow{h\nu} \mathrm{ClOO} \xrightarrow{\Delta} \mathrm{Cl}(^2\mathrm{P}_u) + \mathrm{O}_2(^3\Sigma_g^-, {}^1\Delta_g), \tag{3}$$

Of relevance to halogen-mediated ozone depletion is the ability of OClO to produce photochemically Cl via reactions (2) and (3). The quantum yield for Cl production (Φ_{Cl}) is dependent on phase, with $\Phi_{\mathrm{Cl}} \leq 0.04$ in the gas phase and increasing to unity in low-temperature matrixes [11, 16–36]. Aqueous OClO demonstrates intermediate behaviour with $\Phi_{\mathrm{Cl}} = 0.1$ [37–43]. In addition, Cl production is a bifurcated process in solution, with reactions (2) and (3) contributing 80% and 20% respectively to Φ_{Cl} [44, 45]. The substantial increase in Φ_{Cl} in condensed environments led to the suggestion that this compound may make a significant contribution to stratospheric ozone depletion [9, 11]. However, studies of model polar stratospheric clouds suggest that equilibrium concentrations of OClO on such surfaces are modest, thereby offsetting any increase in Φ_{Cl} [46, 47]. As such, the impact of OClO photochemistry on stratospheric Cl concentrations is expected to be modest. However, the phase dependence of Φ_{Cl} makes this compound an excellent case in which to investigate solvent-dependent photochemical reactivity in an environmental context.

In our attempts to understand at a fundamental level the details behind the phase-dependent reactivity of OClO, we have employed a multidimensional experimental approach that utilizes three spectroscopic techniques: resonance Raman intensity analysis (RRIA), time-resolved resonance Raman (TRRR) and femtosecond pump–probe (FPP) spectroscopy. The synergistic application of these techniques allows for the study of photochemical reactivity from the initial excited-state evolution to the appearance and relaxation of the ground-state products. In this review, we summarize the major findings from our studies and discuss how these results have refined our understanding of the phase-dependent reactivity of OClO. Our work can be partitioned into studies that explore the excited-state dynamics of OClO and studies in which the production and relaxation of the ground-state photoproducts are investigated. Therefore, this article is partitioned accordingly. Although the focus of this manuscript is on the photochemistry of OClO, the questions addressed here are common to many reactions of environmental importance. As such, this work represents not only an attempt to understand OClO photochemistry but also the development of an experimental methodology applicable to a wide range of environmental processes.

2. The excited-state reaction dynamics of OClO

2.1. *Background*

Early spectroscopic studies of OClO focused on its electronic absorption spectrum, and in particular the transition centred at ~360 nm (figure 1(*a*)) [48, 49]. This feature is assigned as the $^2B_1$ (ground) to $^2A_2$ (excited) transition corresponding to the advancement of an electron from an orbital of a_2 symmetry to one of b_1 symmetry [50]. The change in electronic structure weakens the Cl–O bond and decreases the antibonding character between the terminal oxygen atoms. Consequently, the transition exhibits significant vibronic structure involving the

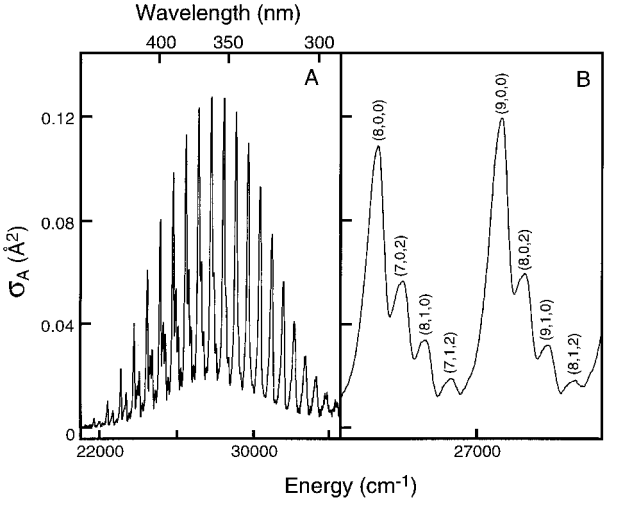

Figure 1. (*a*) Electronic absorption spectrum of chlorine dioxide vapour. Spectra were obtained at a temperature of 293 K. (*b*) Expanded view of the absorption spectrum. Transitions are labeled as (n_1, n_2, n_3) where n is the number of quanta in the excited state along the symmetric stretch (1), bend (2) and asymmetric stretch (3) coordinates.

symmetric-stretch and bend coordinates, with progressions involving the symmetric stretch providing the dominant structure observed in the spectrum (figure 1(*a*)). Of particular interest is the substantial intensity for transitions involving even-overtone excitation along the asymmetric-stretch coordinate (for example, the transitions labelled (7, 0, 2) and (8, 0, 2) in figure 1(*b*)). The ground-state symmetry of OClO is C_{2v} such that fundamental intensity involving the asymmetric stretch is not predicted by symmetry, and this expectation is born out by the absence of such transitions. However, a difference in curvature of the excited-state potential energy surface relative to the ground state can result in overtone intensity along a non-totally symmetric coordinate [51]. Therefore, the presence of transitions having asymmetric-stretch overtone character demonstrates that the ground and excited potential energy surfaces are substantially different along this coordinate. The origin of this intensity was first assigned to the presence of a double-minimum potential in the excited state [48, 49]. This hypothesis was supported by a gas-phase absorption study of OClO seeded into a supersonic jet [52, 53]. In this study, the intensity ratio of transitions involving the symmetric stretch to transitions involving the symmetric and asymmetric stretch was reproduced using a double-minimum potential. However, alternatives to this model have been presented. Brand and coworkers proposed that anharmonic coupling between the symmetric- and asymmetric-stretch coordinates was responsible for the significant intensity of transitions involving the asymmetric stretch [54]. Recent computational studies have provided substantial support for this model [55–58]. Consensus as to the nature of the $^2A_2$ surface along the asymmetric stretch has yet to be reached; however, both models predict that, for gaseous OClO, substantial evolution occurs along the asymmetric-stretch coordinate following photoexcitation.

To study the excited-state relaxation dynamics that occur following OClO photoexcitation, we have used absolute RRIA [59–63]. Numerous excellent reviews are available which discuss the details of this technique [64–66]. In RRIA, absolute Raman scattering cross-sections are measured as a function of excitation wavelength and are used in conjunction with the electronic absorption spectrum to develop a model of the optically prepared excited state. Once determined, this model defines the structural relaxation that occurs on photoexcitation. The connection between excited-state structural evolution and resonance Raman/absorption cross-sections was illustrated by Heller and coworkers using their time-dependent formalism. In this approach, the equations that link the Raman (σ_R) and absorption (σ_A) cross-sections to excited-state structural evolution are as follows [67, 68]:

$$\sigma_R(E_l) = \frac{8\pi E_s^3 E_l e^4 M_{eg}^4}{9\hbar^6 c^4} \int_{-\infty}^{\infty} \partial E_{00}\, H(E_{00}) \left| \int_0^{\infty} \langle f|i(t)\rangle e^{i(E_l+E_i)t/\hbar} D(t)\, dt \right|^2, \quad (4)$$

$$\sigma_A(E_l) = \frac{4\pi e^2 E_l M_{eg}^2}{6\hbar^6 cn} \int_{-\infty}^{\infty} \partial E_{00}\, H(E_{00}) \int_{-\infty}^{\infty} \langle i|i(t)\rangle e^{i(E_l+E_i)t/\hbar} D(t)\, dt. \quad (5)$$

In the above expressions, M_{eg} is the transition length and E_l and E_s are the incident and scattered frequencies respectively. In addition, n is the refractive index of the solvent, E_i is the initial vibrational energy and E_{00} is the energy difference between the ground and excited electronic states. $H(E_{00})$ represents inhomogeneous broadening corresponding to the distribution of E_{00} energies created by differing solvent environments that are static on the timescale of Raman scattering. In our work, this

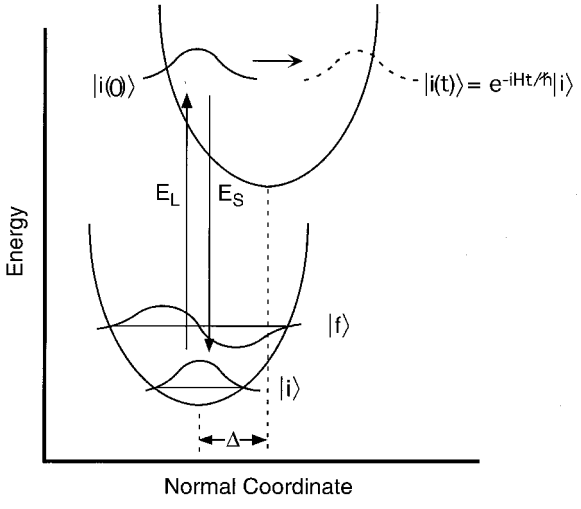

Figure 2. Schematic depiction of the time-dependent formalism for resonance Raman. The incident field (E_l) creates a copy of the ground-state wavepacket on the excited-state potential energy surface $|i(0)\rangle$. Since this initial state is not an eigenstate of the excited state as a result, in this case, of the displacement, Δ, of the excited-state minimum relative to the ground state, the state evolves under the influence of the excited-state Hamiltonian ($|i(t)\rangle$). The Raman and absorption cross-sections are related to the time-dependent overlaps $\langle f|i(t)\rangle$ and $\langle i|i(t)\rangle$ respectively, where $\langle f|$ represents the final state in the scattering process and $\langle i|$ is the initial state.

distribution was modelled as having a Gaussian functional form. $D(t)$ is the homogeneous damping function corresponding to both excited-state population decay and solvent-induced pure dephasing [69]. We have found that a Gaussian model for $D(t)$ best reproduces the absorption and resonance Raman cross-sections of OClO, a result that will be discussed below. The most important components of the above expressions are the time correlators $\langle f|i(t)\rangle$ and $\langle i|i(t)\rangle$. Resonance Raman intensities are dependent on $\langle f|i(t)\rangle$ which represents the overlap of the final state in the scattering process with the initial state propagating under the influence of the excited-state Hamiltonian. As illustrated in figure 2, one can envision this term as a time-dependent Franck–Condon (FC) factor that becomes finite owing to differences in geometry between the ground and excited states. Therefore, the observation of Raman intensity on resonance is evidence that excited-state structural evolution occurs along the corresponding normal coordinate. In analogous fashion, absorption intensity is related to $\langle i|i(t)\rangle$ and corresponds to the time-dependent overlap of the initial ground state with the propagating state. Since the resonance Raman and absorption cross-sections both depend on $|i(t)\rangle$, these spectroscopies can be used in tandem to develop a self-consistent, mode-specific description of the excited-state potential energy surface. Furthermore, this analysis can be performed in a variety of environments, providing the opportunity to examine the dependence of excited-state curvature on environment.

2.2. *RRIA of OClO in the Gas and Condensed Phases*

Figure 3 presents the resonance Raman spectrum of gaseous OClO [62]. The spectrum is dominated by transitions involving the symmetric stretch (ν_1) and bend

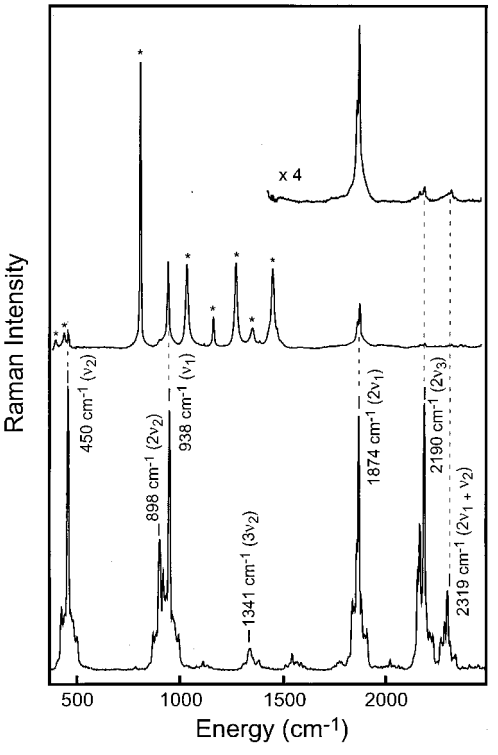

Figure 3. The resonance Raman spectra of OClO dissolved in the gas phase and in cyclohexane. The bottom spectrum is that of gas-phase OClO obtained with an excitation wavelength of 368.9 nm. Transitions corresponding to the symmetric stretch (ν_1) and bend (ν_2) and asymmetric stretch (ν_3) are indicated. The middle spectrum is that of OClO dissolved in cyclohexane. The upper spectrum is an expanded region of the overtone region demonstrating the limited intensity of the asymmetric-stretch overtone transition $(2\nu_3)$. Peaks marked with an asterisk are due to the solvent.

(ν_2). Most interesting is the substantial intensity at 2190 cm^{-1} corresponding to the asymmetric-stretch overtone transition. The asymmetric-stretch coordinate is non-totally symmetric within the C_{2v} point group of ground-state OClO. For non-totally symmetric coordinates, fundamental resonance Raman intensity is not expected by symmetry, and this expectation is born out by the very modest intensity at 1100 cm^{-1}. However, even-overtone transitions involving non-totally symmetric coordinates can demonstrate intensity if the curvature of the excited-state potential energy surface is different from that of the ground state [51]. The observation of asymmetric-stretch overtone intensity immediately demonstrates that the curvatures of excited and ground states along this coordinate differ to a significant extent.

In contrast to the gas phase, the resonance Raman spectrum of OClO in cyclohexane demonstrates only modest asymmetric-stretch overtone intensity. Figure 3 also presents the resonance Raman spectrum of OClO dissolved in cyclohexane [59, 60]. Significant intensity is observed for transitions involving the symmetric-stretch and bend coordinates, demonstrating that excited state structural evolution along these coordinates also occurs in solution. However, the asymmetric-

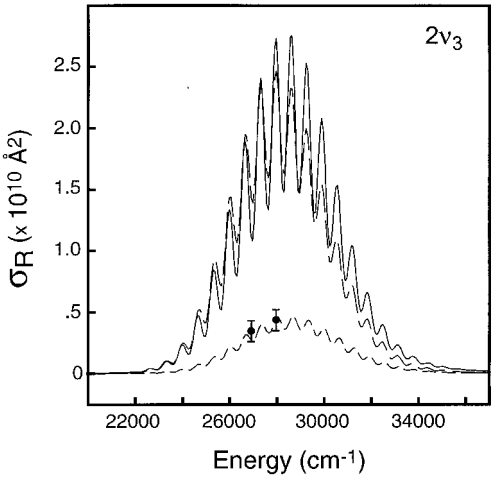

Figure 4. Resonance Raman excitation profile for the asymmetric-stretch overtone transition. Experimental cross-sections are given by the points. The predicted intensity for the overtone transition employing the double-well potential (——), the *ab initio* potential (— — —), and the harmonic potential determined from resonance Raman intensity analysis (– – – –) are presented. Both the double-well and the *ab initio* potentials predict intensity that is roughly an order of magnitude greater than that observed. The observed overtone intensity in cyclohexane is consistent with only a modest reduction in excited-state frequency as described in the text. Similar behaviour is observed for OClO dissolved in water and chloroform.

stretch overtone intensity is extremely modest. This intensity difference relative to the gas phase suggests that the structural evolution that occurs along the asymmetric-stretch coordinate following photoexcitation in the gas phase is significantly restricted in solution. RRIA studies were also performed on OClO dissolved in water and chloroform. In water, no intensity is observed for the asymmetric-stretch overtone transition, consistent with the absence of structural evolution along this coordinate [61]. Similar behaviour was observed in chloroform [63]. The differences in excited-state relaxation dynamics between the gas and solution phase were quantitatively determined by comparing the measured cross-sections for asymmetric-stretch overtone transition to those predicted by either the double-well or the *ab initio* model described above. The results of this analysis for OClO dissolved in cyclohexane are presented in figure 4. The figure demonstrates that both the double-well and *ab initio* surfaces predict substantially greater intensity than what is experimentally observed; therefore, neither gas-phase surface provides an accurate description of the $^2A_2$ state in solution. Instead, the limited asymmetric-stretch overtone intensity was found to be consistent with a modest reduction in frequency from 1100 cm^{-1} in the ground state to ~850 cm^{-1} in the excited state, demonstrating that the substantial evolution that occurs along this coordinate in the gas phase is significantly reduced in solution.

2.3. *The role of symmetry in OClO photochemistry*

Through analysis of the gas and solution-phase absorption and resonance Raman cross-sections, a detailed description of the excited-state structural evolution that occurs following OClO photoexcitation has been developed. In both the gas and

the condensed phases, significant excited-state structural evolution occurs along the symmetric-stretch and bend coordinates. However, the nature of the optically prepared excited state is solvent dependent. The *ab initio* surface predicts that the asymmetric-stretch coordinate undergoes a significant reduction in frequency from $1100\,cm^{-1}$ in the ground state to $419\,cm^{-1}$ in the excited state and that this coordinate is anharmonically coupled to the symmetric stretch. These effects conspire to provide for significant structural relaxation away from the FC region, resulting in a reduction in molecular symmetry from C_{2v} to C_s. Similar behaviour is predicted using the double-well model. In solution, only a slight reduction in frequency on photoexcitation occurs along the asymmetric-stretch coordinate such that structural evolution along this coordinate is minimized. This restricted evolution results in the preservation of C_{2v} symmetry in the excited state when OClO is dissolved in solution.

We have proposed that the preservation of C_{2v} symmetry in the excited state is one reason for the increase in Φ_{Cl} in solution. *Ab initio* calculations have indicated that the reduction of symmetry from C_{2v} to C_s serves to reduce the energy barrier for ClO and O formation such that this pathway becomes most favourable [56]. As such, only for geometries at or near C_{2v} is the production of Cl and O_2 predicted to be appreciable. Experimentally, studies of product formation following gaseous OClO photolysis have shown that the excitation of transitions involving the asymmetric stretch results in roughly a 10-fold reduction in Φ_{Cl} relative to excitation of transitions involving the symmetric stretch exclusively [17]. That is, evolution along the asymmetric stretch serves to promote ClO bond dissociation over Cl production. Our results suggest that similar dynamics contribute to the enhancement of Φ_{Cl} in solution.

Our focus has been on the dynamics that occur on the $^2A_2$ surface; however, it is important to keep in mind that the lower-energy $^2A_1$ and $^2B_2$ excited states also participate in photoproduct production. The sequence of events in OClO photochemistry is believed to be as follows [11]. Internal conversion from the optically prepared $^2A_2$ surface results in production of the $^2A_1$ state, with subsequent production of the lower-energy $^2B_2$ state occurring through $^2A_1$ state internal conversion. Studies of O_2 emission following photoexcitation of OClO in polar and non-polar solvents have demonstrated that in polar solvents, the production of Cl is accompanied by the production of $O_2(^3\Sigma_g^-)$ [70]. However, in non-polar solvents $O_2(^1\Delta_g)$ is predominantly formed. Under C_{2v} symmetry, only the $^2B_2$ state correlates with the $Cl + O_2(^1\Delta_g)$ channel. Therefore, the O_2 emission studies suggest that, in non-polar and polar solvents, Cl is derived from the $^2B_2$ and $^2A_1$ surfaces respectively. Given the similarity of the $^2A_2$ surfaces in water and cyclohexane, the RRIA results taken in combination with the O_2 emission results demonstrate that partitioning between the $Cl + O_2$ channels occurs after decay of the $^2A_2$ surface. The above discussion assumes that C_{2v} symmetry is preserved along the reaction coordinate; however, a reduction in molecular symmetry on either the $^2A_1$ or the $^2B_2$ surface would substantially alter this picture. For example, symmetry reduction could result in the production of the peroxy isomer, ClOO, which is expected to undergo facile decay into Cl and O_2. Therefore, information regarding the rates and quantum yields for photoproduct formation is needed to refine further our description of OClO photochemistry (see below).

2.4. *Solvent response to OClO photoexcitation*

Using absolute resonance Raman intensities, it is possible to partition spectral broadening into its homogeneous and inhomogeneous contributions [64, 66]. In our studies, we have found that the homogeneous linewidth (Γ) is essentially the same in all solvents studied to date, having an average value of $\sim$90 cm^{-1} corresponding to a total dephasing time of $\sim$60 fs. The homogeneous linewidth contains contributions from both excited-state population decay and solvent-induced pure dephasing [69]:

$$\Gamma = \frac{1}{T_2} = \frac{1}{2T_1} + \frac{1}{T_2^*}. \tag{6}$$

In the above expression, T_2 is the total dephasing time, T_1 is the excited-state lifetime and T_2^* is the timescale for solvent-induced pure dephasing. Recent fluorescence cross-section measurements and FPP studies have established that T_1 is $\sim$200 fs [63, 71]. Comparison of this time with the total dephasing time ($\sim$60 fs) demonstrates that solvent-induced pure dephasing makes the dominant contribution to the homogeneous linewidth. Therefore, the solvent invariance of Γ suggests that the solvent dynamics responsible for dephasing occur on the same timescale in all solvents studied to date.

We have proposed that the solvent invariance of Γ reflects the dominance of non-polar or mechanical solvation in response to OClO photoexcitation. The motivation behind this idea is as follows. *Ab initio* studies predict that the dipole moment (μ) of OClO changes by only $\sim$0.1 D on photoexcitation and that the direction of the dipole moment remains relatively unchanged [57]. This small change in solute electronic distribution is expected to result in a modest solvent dielectric response. In contrast, the significant displacement along the symmetric-stretch and bend coordinates results in a substantial geometry change on photoexcitation. Specifically, the excited-state equilibrium geometry corresponds to an increase in Cl–O bond length of $\sim$0.2 Å and an O–Cl–O bond angle decrease of $\sim$9° relative to the ground state [61]. Therefore, we would expect repulsive solvent–solute interactions to be dramatically altered by this change in geometry such that mechanical solvation dynamics should make the dominant contribution to the solvent response. In support of this hypothesis, we have shown that the viscoelastic continuum (VC) model of non-polar solvation as outlined by Berg is capable of reproducing the homogeneous linewidth [72–74].

In the VC model, the solute is approximated as a spherical cavity located within the solvent, modelled as a viscoelastic continuum. Before excitation, a balance exists between the force applied by the continuum directed towards collapse of the solute cavity and the restoring force applied to the continuum by the solute opposing cavity collapse. Photoexcitation of the solute initiates a change in molecular size and a corresponding change in the force applied by the solute to the cavity boundary, and the size of the solute cavity will therefore change to restore equilibrium. The solvent is modelled as isotropic, and the solvent response is separated into two components, one that occurs in the same direction of the applied force (known as the compressive strain) and another that occurs in directions perpendicular to the applied force (known as the shear strain). Correspondingly, the solvent response is described by the compressive and shear moduli for the solvent denoted by K and G respectively. For a force resulting in deformation of the material only in the same direction as the applied force, the ratio of the stress to the strain in that direction is called the wave modulus, M, and is given by

$$M = K + \tfrac{4}{3}G. \tag{7}$$

The moduli G, K and M describing the viscoelastic response of the medium are time dependent. However, the dynamics of interest occurs on a relatively short timescale such that one can consider only the short-time, solid-like response of the medium so that only the high-frequency moduli $G\infty$, $K\infty$, and $M\infty$) are needed. By solving the appropriate viscoelastic equations of motion, Berg has used these moduli to calculate the solvent response $(R(t))$ [72, 73]:

$$R(t) = (1-f)\,\mathrm{e}^{-t/\tau_{\mathrm{ph}}}\left[\cos\left(\frac{t}{\beta\tau_{\mathrm{ph}}}\right) - \beta\sin\left(\frac{t}{\beta\tau_{\mathrm{ph}}}\right)\right] + f\,\mathrm{e}^{-t/\tau_{\mathrm{st}}} \tag{8}$$

with

$$\beta^2 = 3\frac{M\infty + (K_{\mathrm{s}} - K\infty)}{M\infty - 3(K_{\mathrm{s}} - K\infty)}, \tag{9}$$

$$f = \frac{\frac{4}{3}G\infty}{K_{\mathrm{s}} + \frac{4}{3}G\infty}, \tag{10}$$

$$\tau_{\mathrm{ph}} = \frac{1+\beta^2}{2\beta^2}\tau_{\mathrm{l}}, \tag{11}$$

$$\tau_{\mathrm{l}} = r_{\mathrm{c}}\left(\frac{\rho}{M\infty}\right)^{1/2}, \tag{12}$$

$$\tau_{\mathrm{st}} = \frac{\eta/G\infty}{1-f}. \tag{13}$$

In the above equations, τ_{l} is the time for longitudinal sound waves to travel a distance of one cavity radius, K_{s} is the effective compressive modulus of the solute and ρ is the solvent density. In addition, r_{c} is the cavity radius which is taken to be 3 Å. Equation (8) is valid in the limit that only phonon-induced solvation is rapid compared with the structural relaxation of the solvent. In this limit, the solvent response is partitioned into two parts, a phonon-induced response (the term with the $1-f$ prefactor in equation (8)) and a slower, structural relaxation of the solvent.

In the limit of linear response, $R(t)$ can be equated to $C(t)$, the normalized correlation function that describes the solvent-induced fluctuations in the energy gap between ground and excited state of the solute:

$$C(t) = \frac{\langle \delta U(t)\,\delta U(0)\rangle}{\langle \delta U^2\rangle}. \tag{14}$$

In the above expression, U is the energy gap between ground and excited states, and $\delta U(t) = U - \langle U\rangle$ is the fluctuation of the energy gap from its equilibrium value. Assuming that the linear response limit is correct, then $R(t)$ as described by VC theory can be used to determine $C(t)$, with this term subsequently used to determine the functional form for homogeneous dephasing, $D(t)$. Our determination of $D(t)$ follows closely the Brownian oscillator development presented by Mukamel in which solvent-induced dephasing is incorporated into the expression for Raman or absorption cross-section by $D(t) = \mathrm{e}^{-g(t)}$ where [75]

$$g(t) = \int_0^t \mathrm{d}\tau_1 \int_0^{\tau_1} \mathrm{d}\tau_2\, \langle \delta U(\tau_2)\,\delta U(0)\rangle. \tag{15}$$

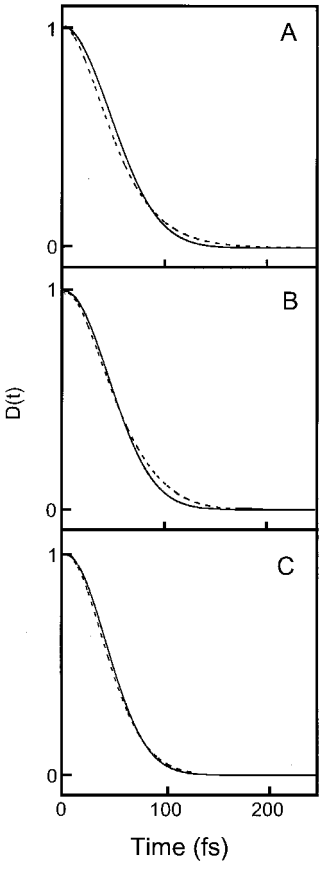

Figure 5. Comparison between the homogeneous linewidth, $D(t)$, determined from RRIA and that predicted using the VC treatment described in the text. Results are presented for (*a*) cyclohexane, (*b*) water and (*c*) chloroform [63]. In each panel, the RRIA result is given by the full curve and the VC result is given by the broken curve.

Thus, by knowing $C(t)$ and equating the variance of the fluctuations or Δ^2 to $\langle \delta U^2 \rangle$, a functional form for $g(t)$ and subsequently $D(t)$ can be obtained. Using the expression for $R(t)$ provided in equation (8), $g(t)$ becomes

$$g(t) = (1-f)\frac{\Delta^2 \tau_{\mathrm{ph}}^2}{\hbar^2(1+1/\beta^2)}\left\{1 - \mathrm{e}^{-t/\tau_{\mathrm{ph}}}\left[\cos\left(\frac{t}{\beta\tau_{\mathrm{ph}}}\right) + \beta \sin\left(\frac{t}{\beta\tau_{\mathrm{ph}}}\right)\right]\right\}$$
$$+ f\frac{\Delta^2\tau_{\mathrm{st}}^2}{\hbar^2}\left(\frac{t}{\tau_{\mathrm{st}}} + \mathrm{e}^{-t/\tau_{\mathrm{st}}} - 1\right). \qquad (16)$$

Although the above expression looks complex, it is important to keep in mind that the only variable is Δ since the other parameters are defined by the compressive and sheer moduli of the solvent. A comparison between $D(t)$ as determined by RRIA for OClO dissolved in cyclohexane, water and chloroform, and the VC prediction is presented in figure 5 [63]. Reasonable agreement between the model and the experimental $D(t)$ was obtained with $\Delta = 155$, 150 and 160 cm^{-1} in cyclohexane, water and chloroform respectively. Most impressive is the ability of the VC model to

reproduce the solvent invariance of $D(t)$, suggesting that non-polar solvation dynamics is indeed responsible for solvent-induced pure dephasing. Molecular dynamics studies have shown that the repulsive interactions that lead to non-polar solvation are dominated by a few molecules located in the first solvent shell [76, 77]. Current interest in this area involves connecting the microscopic picture of non-polar solvation derived from computation studies with the macroscopic picture provided by VC theory.

One final question concerns the solvent–solute interactions responsible for the restricted evolution along the asymmetric-stretch coordinate. One answer to this question is found in the increase in the inhomogeneous linewidth with an increase in solvent polarity. Specifically, the standard deviation that characterizes the Gaussian solvent-site distribution increases from $140\,cm^{-1}$ in cyclohexane to $220\,cm^{-1}$ in chloroform to $280\,cm^{-1}$ in water. This evolution in inhomogeneous broadening suggests that dielectric solvent–solute interactions are operative on longer timescales (>200 fs) relative to the dynamics responsible for homogeneous broadening. The contribution of dielectric interactions to slower-time solvent dynamics can also be understood by considering the essential invariance of the molecular dipole moment following photoexcitation. This modest change in molecular dipole moment results in an equilibrium solvent configuration for the ground state that is the same for the excited state. As such, any change in dipole moment must overcome the stabilization provided by the solvent. Since the largest change in dipole moment occurs with displacement along the asymmetric stretch, it is perhaps not surprising that this coordinate is affected by the presence of solvent.

3. OClO photoproduct formation dynamics

3.1. *Background*

As mentioned in the introduction, recent studies of OClO have been motivated by its potential role in stratospheric ozone depletion due to its ability to generate Cl photochemically. To evaluate the environmental impact of OClO and other halooxides, it is necessary to identify the available photochemical pathways and how partitioning between pathways is dependent on environment. Towards this end, Simon and coworkers initiated a set of picosecond transient absorption studies of OClO in several solvents to monitor photoproduct-formation dynamics [37, 38, 78]. These studies lead to the conclusion that following photoexcitation both ClO/O and Cl/O_2 are produced. These authors established that the quantum yield for Cl formation (Φ_{Cl}) is 0.1 in water, substantially greater than in the gas phase. It was also demonstrated that, in water and sulphuric acid, a finite percentage of the ClO and O primary photofragments undergo geminate recombination on the nanosecond timescale; however, in polar aprotic solvents and alcohols recombination was not observed [38]. With respect to the Cl/O_2 channel, singlet oxygen emission studies suggested that most of the Cl formed originated from decomposition of ground-state ClOO, the structural isomer of OClO [70]. From this result in combination with the *ab initio* study of Jafri *et al.*, which predicted the presence of a ClOO absorption band in the visible region of the spectrum, Simon and coworkers suggested that the evolution in optical density observed in their studies was consistent with the production of ClOO [38, 78, 79].

In recent years, femtosecond transient absorption studies have refined our understanding of the early-time photoproduct formation dynamics following OClO

photoexcitation. Femtosecond studies performed by Chang and Simon on aqueous OClO mapped out the evolution in optical density evolution that occurs from 350 to 700 nm following OClO photoexcitation [80]. This evolution was interpreted in terms of ClOO formation and vibrational relaxation in agreement with the results of the picosecond transient absorption studies outlined above. Later experiments by Keiding and coworkers called into question this interpretation of the pump–probe dynamics [41]. These authors performed an FPP study in which the optical-density evolution was also monitored at 260 and 400 nm such that dynamics associated with ClOO/ClO and OClO respectively were monitored. The evolution in optical density at 260 nm was demonstrated to be more consistent with ClO decay. Furthermore, using a kinetic argument combined with the absolute changes in optical density observed at both 260 and 400 nm, the decay in ClO was correlated with the reformation of OClO. This observation led to the hypothesis that the primary ClO and O photofragments undergo subpicosecond geminate recombination resulting in the production of vibrationally hot OClO. In this model, the optical density evolution observed in the visible region of the spectrum was due to the formation and vibrational relaxation of OClO. This study also demonstrated that a precursor to Cl formation was formed and underwent decomposition within 25 ps. Additional FPP studies by Keiding and coworkers further explored the vibrational relaxation dynamics of OClO and suggested that, following recombination, excess vibrational energy was deposited along the asymmetric stretch with the majority of energy exchange with the solvent occurring through this coordinate [40].

In order to differentiate between the two photochemical models presented above, experiments that could unequivocally determine the identity of those species formed following OClO photoexcitation were needed. With this motivation, we employed TRRR spectroscopy to study the photoproduct formation and vibrational relaxation dynamics of OClO in solution. This spectroscopic technique is capable of providing kinetic information through the temporal evolution in scattered intensities and structural information characteristic of a vibrational spectroscopy. The results from this work are outlined below.

3.2. *Geminate recombination of the OClO primary photoproducts*

To monitor the solvent-dependent photoproduct and vibrational relaxation dynamics of OClO, we have performed TRRR studies in a variety of polar protic and polar aprotic solvents [81–83]. Our first studies were performed in water to connect with the body of existing FPP work [81, 82]. In these studies, the temporal evolution in the resonance Raman spectrum following excitation at 390 nm was monitored using a probe beam at the same wavelength. The results of this study are summarized in figure 6(*a*). The spectra presented in this figure represent the difference between the probe spectrum in the presence and absence of photolysis. At 0 ps delay, when the pump and probe are overlapped in time, significant depletion in OClO scattering is observed consistent with a reduction in ground-state OClO concentration due to photolysis. As the temporal delay between the pump and probe increases, the OClO depletion intensity decreases up to 20 ps after which time further evolution was not observed out to the longest delays investigated (500 ps). This evolution in depletion intensity demonstrates that ground-state OClO is re-formed and directly confirms the geminate recombination model discussed above. Comparison of the depletion at zero delay with the persistent depletion at later delays

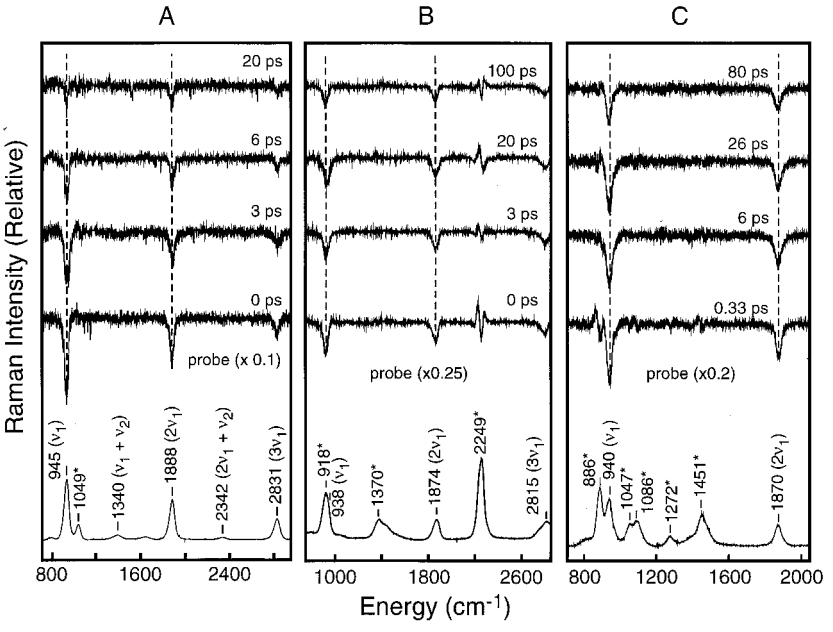

Figure 6. Time-resolved Stokes spectra for aqueous (*a*) OClO, (*b*) OClO dissolved in acetonitrile and (*c*) OClO dissolved in ethanol. Spectra were obtained with degenerate pump and probe wavelengths of 390 nm. The 0 ps Stokes spectrum demonstrates depletion in OClO scattering due to photolysis. As the probe is delayed relative to the pump, the depletion amplitude decreases owing to OClO reformation via geminate recombination of the ClO and O photoproducts. The peaks marked with an asterisk in the probe-only spectrum are due to the solvent, and in (*a*) the peak at 1049 cm^{-1} is due to NO_3^- added as an internal scattering standard.

established that geminate recombination occurs to a significant extent in water, with a quantum yield of 0.8 ± 0.1.

The kinetics of ground-state OClO re-formation by geminate recombination were determined by plotting the intensity of the symmetric-stretch fundamental transition (945 cm^{-1}) as a function of time (figure 7(*a*)). The evolution in intensity was best modelled by a sum of two exponentials having time constants of 0.15 ± 0.1 ps (i.e. instrument response limited) and 9.2 ± 3.5 ps. A third, long-time component (10 000 ps, fixed) was included to reproduce the persistent depletion in scattering intensity at long delays. These time constants were interpreted as follows. Subpicosecond geminate recombination of the primary ClO and O photofragments results in the production of vibrationally excited OClO which undergoes intermolecular vibrational relaxation on the ~9 ps timescale. Assignment of the early-time depletion recovery to geminate recombination is consistent with the subpicosecond recombination times observed in other systems [84]. To determine whether the 9 ps recovery time constant was indeed due to vibrational relaxation, time-resolved anti-Stokes experiments were performed, with representative results presented in figure 8(*a*). The figure demonstrates that intensity corresponding to the symmetric-stretch fundamental and overtone transitions is observed. The temporal evolution in symmetric-stretch fundamental anti-Stokes intensity is presented in figure 7(*b*). Best fit to these data by a sum of two exponentials resulted in appearance

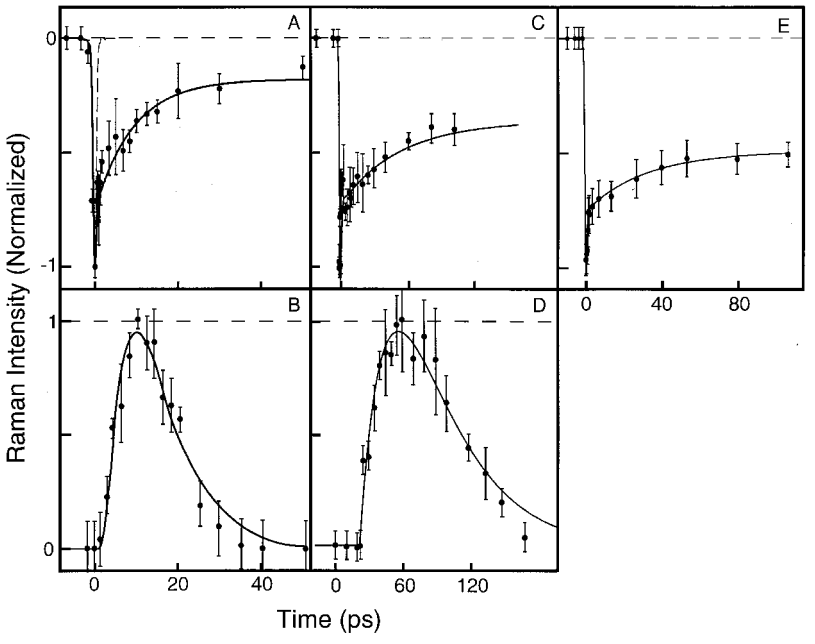

Figure 7. (*a*) Intensity of the aqueous OClO symmetric-stretch fundamental Stokes transition as a function of time. Best fit to the data by a sum of exponentials convolved with the instrument response (full curve) was obtained with time constants (with normalized amplitude in parentheses) of 0.15 ± 0.1 ps (0.65), 9.2 ± 3.5 ps (0.27) and 10 000 ps representing the long-time offset in intensity (0.08). (*b*) Intensity of the aqueous OClO symmetric stretch anti-Stokes fundamental transition as a function of time. Best fit to the data by a sum of two exponentials convolved with the instrument response (full curve) was obtained with an appearance time constant (with normalized amplitude in parentheses) of 5.2 ± 1.5 ps (0.5) and a decay time constant of 9.2 ± 1.7 ps (0.5). (*c*) Temporal evolution for symmetric-stretch overtone Stokes transition of OClO dissolved in acetonitrile. Best fit to the data by a sum of exponentials convolved with the instrument response (full curve) was obtained with time constants (with normalized amplitude in parentheses) of 0.15 ± 0.1 ps (0.8), 33.0 ± 8.1 ps (0.08) and 10 000 ps representing the long-time offset in intensity (0.12). (*d*) Intensity of the symmetric stretch anti-Stokes fundamental transition as a function of time. Best fit to the data by a sum of two exponentials convolved with the instrument response (full curve) was obtained with an appearance time constant (with normalized amplitude in parentheses) of 33.7 ± 4.4 ps (0.5) and a decay time constant of 36.7 ± 4.4 ps (0.5). (*e*) Temporal evolution for the symmetric-stretch overtone Stokes transition of OClO dissolved in ethanol. Best fit to the data by a sum of exponentials convolved with the instrument response (full curve) was obtained with time constants (with normalized amplitude in parentheses) of 0.3 ± 0.1 ps (0.82), 31.0 ± 10 ps (0.06) and 10 000 ps representing the long-time offset in intensity (0.12).

and decay times of 5.2 ± 1.5 ps and 9.2 ± 1.7 ps respectively. The agreement between the ~9 ps Stokes appearance and anti-Stokes decay time constants establishes that the intensity evolution that occurs on this timescale is due to vibrational relaxation.

Our first solvent-comparative study involved the photochemistry of OClO in water and in acetonitrile [82]. FPP studies of I_2^- photodissociation and recombination have shown that geminate-recombination quantum yields are significantly reduced in acetonitrile relative to water, presumably because of the absence of intermolecular hydrogen bonding in this polar, aprotic solvent [85]. Figure 6(*b*)

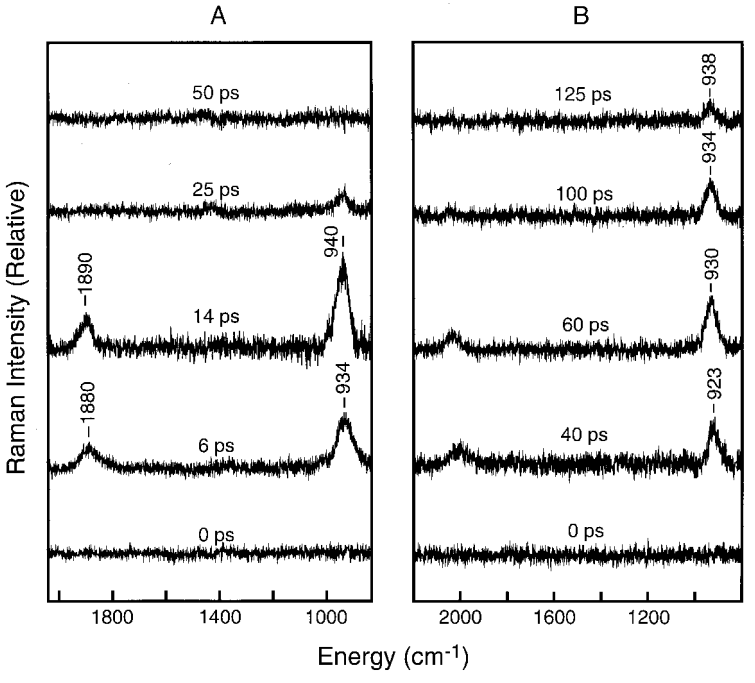

Figure 8. Time-resolved anti-Stokes spectra for OClO dissolved in (*a*) water and (*b*) acetonitrile. Spectra were obtained with degenerate pump and probe wavelengths of 390 nm. Intensity is observed for the fundamental and overtone transitions of OClO consistent with excess vibrational energy being deposited along this coordinate following geminate recombination.

presents representative time-resolved resonance Raman Stokes spectra of OClO dissolved in acetonitrile. At first appearance, the temporal evolution in scattered intensity observed in this solvent is similar to that in water. The extent of OClO scattering depletion observed at zero time decreases with an increase in delay; however, the extent of depletion at later times is much greater. Consistent with this observation, comparison of the initial depletion with that which persists at later time establishes that the geminate-recombination quantum yield is 0.55 ± 0.05 in acetonitrile. Furthermore, evolution occurs over a substantially longer timescale in acetonitrile relative to water. Figure 7(*c*) presents the temporal evolution in the OClO symmetric-stretch overtone intensity as a function of time. The evolution observed here is similar to that in water with the extent of depletion decreasing at longer delays. Similar to the behaviour observed in water, the OClO scattering depletion undergoes biphasic recovery with time constants of 0.15 ± 0.1 ps (i.e. instrument response limited), and 33.0 ± 8.1 ps. Figure 8(*b*) presents time-resolved anti-Stokes spectra of OClO dissolved in acetonitrile, and the intensity of the symmetric-stretch anti-Stokes fundamental transition as a function of time in this solvent is presented in figure 7(*d*). Both figures demonstrate that the appearance and decay of anti-Stokes intensity occurs over a much longer timescale in acetonitrile relative to water. This observation demonstrates that the vibrational relaxation occurs over longer times in acetonitrile. Best fit to the temporal evolution of anti-Stokes intensity in acetonitrile by a sum of two exponentials convolved with the

instrument response results in appearance and decay time-constants of 33.7 ± 4.4 ps and 36.7 ± 4.6 ps respectively. The excellent agreement between the later-time Stokes depletion recovery and anti-Stokes decay time constants demonstrates that vibrational relaxation occurs with a time constant of ~35 ps in acetonitrile.

We have also investigated the photochemistry of OClO in ethanol [83]. The time-resolved Stokes spectra obtained in this solvent are presented in figure 6(*c*). Similar to the behaviour observed in water and acetonitrile, depletion is observed for all OClO transitions, with the extent of depletion decreasing at longer delays consistent with OClO re-formation and vibrational relaxation. However, the extent of depletion in this solvent at later times is much greater than what was observed in water, yet similar to the extent of depletion that was observed in acetonitrile. The evolution in the OClO symmetric-stretch overtone intensity as a function of time is presented in figure 7(*e*). This figure demonstrates that, similarly to the other solvents studied, depletion recovery is biphasic occurring with time constants of 0.3 ± 0.1 ps and 31 ± 10 ps. Comparison of the initial depletion with that which persists at long delays establishes that the geminate recombination quantum yield in ethanol is 0.5 ± 0.1, essentially identical to the behaviour observed in acetonitrile.

Comparison of the TRRR results presented above firmly established that the primary ClO and O photofragments undergo geminate recombination to re-form ground-state OClO. Specifically, the recovery of depletion intensity confirms that the re-formation of ground-state OClO is a dominant feature of solution-phase OClO photochemistry. Subpicosecond OClO reformation is observed in all three solvents, suggesting that the geminate-recombination rate is insensitive to the nature of the solvent. However, the efficiency of recombination is clearly solvent dependent as evidenced by the decrease in the recombination quantum yield from 0.9 in water to 0.55 in acetonitrile and ethanol. This behaviour has been correlated with the extent of solvent association, where greater association provides for a stronger solvent cage and thereby a larger geminate-recombination quantum yield. This hypothesis was tested in a comparative TRRR study of OClO dissolved in ethanol and 2,2,2-trifluoroethanol (TFE) [83]. The idea behind this work was to vary the hydrogen-bonding strength of the solvent through halogen substitution and to monitor the effect of this perturbation on geminate recombination. We found that the geminate-recombination quantum yield was significantly reduced in TFE, consistent with the propensity of this solvent to exist in monomeric form compared with the polymeric structures favoured in ethanol [86–88]. Therefore, it appears that solvent association via hydrogen bonding is one important factor in defining geminate-recombination quantum yields. However, the similarity in the geminate-recombination quantum yields in acetonitrile and ethanol demonstrates that hydrogen bonding is not the only factor. It should be noted the geminate-recombination rate in TFE was not instrument response limited, a result that was attributed to interaction of the photofragments with the solvent as evidenced by spectral evolution in the TRRR spectra.

3.3. *The vibrational relaxation dynamics and OClO*

The anti-Stokes studies presented above demonstrate that the formation of OClO via geminate recombination of the primary photofragments is accompanied by the deposition of excess vibrational energy into the molecule. Anti-Stokes intensity corresponding to the OClO symmetric-stretch fundamental and overtone transitions is observed consistent with vibrational excitation along this degree of freedom.

Vibrational relaxation is also evidenced by the increase in symmetric-stretch fundamental transition frequency with delay due to anharmonicity. Although anti-Stokes intensity is observed in both solvents, the timescales over which evolution is observed are markedly different. Specifically, the appearance and decay of anti-Stokes intensity occurs over a much longer timescale in acetonitrile relative to water. This can be seen clearly in figure 7, which presents the integrated intensity of the symmetric-stretch fundamental anti-Stokes transition in water and in acetonitrile as a function of time. As mentioned above, the anti-Stokes intensity has an appearance time of 5.2 ± 1.5 ps and decay time of 9.2 ± 1.7 ps in water, with corresponding times of 33.7 ± 4.4 ps and 36.7 ± 4.6 ps in acetonitrile. The decay times observed in both solvents agree with the recovery time constants obtained in the analysis of the Stokes spectra, confirming the assignment of these time constants to vibrational relaxation.

Perhaps the most intriguing result obtained in our studies is that the sub-picosecond recovery of symmetric-stretch Stokes intensity is not reflected by a similar, rapid appearance of anti-Stokes intensity. Although this effect could be due to small anti-Stokes cross-sections at the probe wavelength employed, computational studies suggest that the anti-Stokes scattering cross-sections should be appreciable even at elevated molecular temperatures [82]. Therefore, the discrepancy between the rapid OClO Stokes recovery and the slower appearance of anti-Stokes intensity suggests that geminate recombination of the ClO and O fragments results in the production of OClO with minimal vibrational excitation along the symmetric-stretch coordinate. This conclusion is consistent with FPP studies of aqueous OClO that have been interpreted in terms of geminate recombination resulting in energy deposition along the asymmetric-stretch coordinate [40]. Therefore, the current model for OClO vibrational relaxation following geminate recombination is that, immediately following geminate recombination, OClO is produced with excess vibrational energy deposited along the asymmetric-stretch coordinate.

The vibrational relaxation dynamics of OClO provides insight into the interplay between energy dissipation to the solvent and intramolecular vibrational energy redistribution (IVR). Solution-phase vibrational relaxation studies have been dominated by diatomic systems in which IVR is not operative [85, 89, 90]. Triatomic systems such as OClO represent the simplest class of molecules in which the effect of intermolecular energy dissipation on IVR can be studied. Computational studies of the anti-Stokes symmetric-stretch fundamental and overtone transitions found that the maximum internal temperature reached in both water and acetonitrile is $\sim$4500 K, corresponding to a vibrational-energy content of 9500 cm^{-1}. Given that 17 000 cm^{-1} of vibrational energy is available to OClO following recombination, this result demonstrates that $\sim$7500 cm^{-1} is lost to the solvent through energy exchanged between the solvent and the asymmetric-stretch coordinate. Following or concomitant with this initial relaxation, IVR occurs with a time constant of $\sim$5 ps in water and $\sim$20 ps in acetonitrile; therefore, the timescale for energy deposition along the symmetric-stretch coordinate is solvent dependent. In addition, the similarity in maximum solute temperature determined through analysis of the anti-Stokes intensities suggests that similar levels of the asymmetric-stretch vibronic manifold must be reached before IVR takes place. It has been proposed that, at early times, the high degree of OClO excitation results in the predominance of a local-mode description of the coordinates favoring energy localization into a single Cl–O bond [82]. With energy dissipation, a transition from local to normal coordinates occurs,

promoting IVR. The bifurcation of normal modes at high excitation energies and the effect of bifurcation on intramolecular energy flow including the generation of energy 'bottlenecks' has been recognized [91–93].

3.4. *Theoretical models for vibrational relaxation in OClO*

Given the solvent-dependent vibrational relaxation dynamics as evidenced by the Stokes recovery and anti-Stokes decay kinetics presented above, current interest involves understanding the nature of the solvent–solute coupling that results in this behaviour. In particular, the description of OClO vibrational relaxation presented above suggests that much of this solvent dependence is dominated by differences in the rate of energy deposition into the solvent via the asymmetric-stretch coordinate. Is solvent–solute coupling involving the asymmetric stretch solvent dependent, and if so is this dependence sufficient to explain the solvent dependence of the vibrational-relaxation rate? To address these questions, Poulsen and coworkers have recently reported a theoretical study of OClO vibrational relaxation in water using a semiclassical golden-rule formulation [94]. In this approach, all the vibrational modes of the relaxing solute are treated quantum mechanically, while the solvent degrees of freedom are treated classically. The effect of the solvent on the solute is included via a coupling term, which involves the force (f) exerted by the solvent on the solute vibrational coordinate. Determination of the vibrational relaxation rate is then performed by calculating the force–force autocorrelation function $(\langle f(t)f(0)\rangle)$ via molecular dynamics. Poulsen and coworkers have focused on energy relaxation out of the asymmetric-stretch coordinate, and in particular on the transition rate out of the first excited vibrational state along this coordinate. The total relaxation rate obtained from this approach, $0.11\,\mathrm{ps}^{-1}$, is remarkably close to the rate obtained by this same group in their FPP studies [40]. Finally, the authors found strong coupling between the asymmetric and symmetric stretch coordinates, which accounted for an appreciable portion of the total relaxation rate for the first excited vibrational state along the asymmetric stretch. This finding supports the hypothesis that IVR dynamics between these two coordinates is responsible for the observed delay in the appearance of anti-Stokes intensity involving the symmetric stretch.

Benjamin and coworkers have taken a similar approach in studying OClO vibrational-relaxation dynamics in water as well as a variety of other solvents [95]. In particular, these authors were interested in addressing the solvent-dependent vibrational relaxation dynamics observed in our TRRR studies. Employing molecular dynamics, the authors followed both vibrational-energy relaxation to the solvent and redistribution of this energy among the OClO modes after an initial deposition of energy into the symmetric-stretch and asymmetric-stretch coordinates. Different regions of the ground-state vibronic manifold were accessed in the calculations by altering the amount of energy initially deposited into OClO. The average relaxation times obtained from the non-equilibrium calculations were 7.1, 34.0 and 33.8 ps for water, acetonitrile and ethanol respectively. These results are in excellent agreement with the experimental relaxation times presented above and are also consistent with results from pump–probe studies [40, 82].

Using an approach similar to that described above, Benjamin and coworkers also calculated the solvent-dependent force autocorrelation function $(\langle f(t)f(0)\rangle)$ and corresponding power spectrum for the solvents of interest. It was determined that the most important contribution to the solvent-dependent vibrational relaxation dynamics was the frictional force exerted by solvent. They also concluded that the

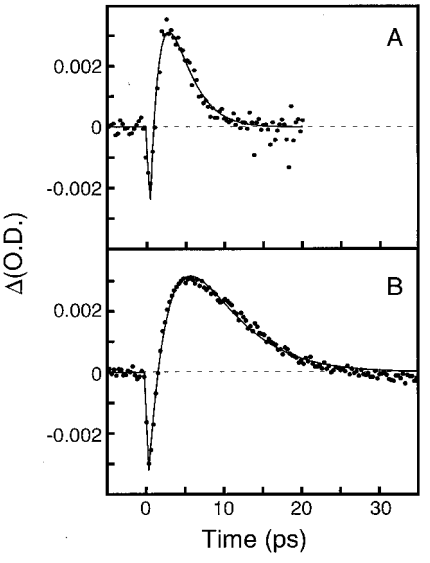

Figure 9. FPP data for OClO dissolved in (*a*) water and (*b*) D_2O using pump and probe wavelengths of 400 nm and 600 nn respectively. Best fit to the data by a sum of two exponentials convolved with the instrument response function resulted in time constants of 1.7 ± 0.1 ps and 1.9 ± 0.1 ps in H_2O and 3.1 ± 0.4 ps and 4.9 ± 0.7 ps in D_2O. Errors represent 1 standard deviation from the mean value determined from three measurements.

greater force in water is due to the extensive hydrogen-bonding network in water compared with the other two solvents. As a test of this hypothesis, the authors proposed that, if the relaxation dynamics of OClO were studied in D_2O, the shift in the power spectrum to lower frequencies accompanying isotopic substitution should reduce the state-to-state transition rate by a factor of 2 relative to water. This hypothesis was recently tested in our laboratory. Specifically, the vibrational-relaxation dynamics of OClO dissolved in H_2O and D_2O was monitored at 600 nm following photoexcitation at 400 nm. At this probe wavelength, the evolution in optical density is dominated by dynamics associated with OClO vibrational relaxation [40, 82]. Figure 9 presents the results of this study. Following an initial reduction in optical density corresponding to stimulated emission [71, 96], an increase and subsequent decay in optical density is observed as a result of the appearance and decay of vibrationally excited OClO. Clearly, the evolution in optical density in D_2O is significantly slower relative to H_2O. In quantitative terms, the later time rise and decay time constants were determined to be 1.7 ± 0.1 ps and 1.9 ± 0.1 ps in H_2O, and these times increase to 3.1 ± 0.4 ps and 4.9 ± 0.7 ps in D_2O. As predicted, the vibrational relaxation rate is approximately two times slower in D_2O compared with H_2O ($\sim 0.2\ ps^{-1}$ vs. $\sim 0.5\ ps^{-1}$), consistent with dielectric friction playing an important role in defining the vibrational relaxation dynamics of OClO.

The simulations also provide some detailed predictions regarding the IVR mechanism in OClO. In water, initial energy flow between the symmetric and asymmetric stretches was observed, followed by energy flow into the bend. Furthermore, the rate of energy deposition into the bend was found to increase with an increase in initial vibrational excitation. Interestingly, this behaviour was

found to be solvent dependent. In acetonitrile and ethanol, energy flow between the symmetric stretch and bend coordinates is substantial, while energy deposited along the asymmetric stretch was channelled into the solvent with little exchange. The authors postulate that these solvent-dependent IVR dynamics could be responsible for the apparent solvent-dependent IVR dynamics outlined above.

3.5. *The Production of Cl*

Although it has been established that the quantum yield for Cl formation following the photoexcitation of aqueous OClO is 0.1, the mechanism by which Cl is produced and the role the environment plays in defining this mechanism have remained unclear. In particular, the role of ClOO in Cl production has only recently been addressed [45, 97, 98]. The TRRR studies described above did not provide evidence for ClOO formation following OClO photoexcitation [82]. Specifically, no positive intensity was observed in the difference spectra consistent with photoproduct formation. However, the absence of ClOO scattering in these experiments could simply be the result of limited resonance given the 390 nm excitation wavelength employed. Studies of ClOO in ice have shown that this species has a strong absorption band centred at ~250 nm [36, 99, 100]. Therefore, we performed two-colour TRRR studies of aqueous OClO employing pump and probe wavelengths of 390 and 260 nm respectively [45]. This probe wavelength falls within the absorption band of ClOO, and thus resonance enhancement of the Raman scattering cross-section is expected at this probe wavelength.

Figure 10(*a*) presents TRRR Stokes difference spectra of aqueous OClO [45, 97]. At 0 ps, negative intensity is observed for transitions corresponding to OClO consistent with depletion of the ground state due to photolysis, similar to the behaviour observed in our previous TRRR experiments. As the delay between the pump and probe is increased, the OClO depletion decreases, consistent with ground-state OClO production via geminate recombination. The temporal evolution in OClO symmetric-stretch fundamental transition intensity (945 cm^{-1}) was found to be similar to our earlier results presented above. More interesting is the presence of positive intensity at 1442 cm^{-1}, demonstrating that ClOO is produced following aqueous OClO photolysis. This intensity corresponds to the O–O stretch coordinate of ClOO [32, 33, 101, 102]. To solidify this assignment, TRRR spectra at lower frequency were obtained, and intensity corresponding to the ClOO bend (428 cm^{-1}) was also observed [45]. To study the kinetics of ClOO production and decay, the integrated intensity of the 1442 cm^{-1} transition was plotted as a function of time as shown in figure 11(*a*). These data demonstrate that ClOO production is significantly delayed relative to OClO production, with the intensity of the O–O stretch reaching a maximum at ~100 ps. Consistent with this observation, best fit to these data by a sum of two exponentials convolved with the instrument response resulted in appearance and decay time constants of 27.9 ± 4.5 ps and 398 ± 50 ps. These time constants are assigned to the production of ground-state ClOO and thermal decomposition resulting in the formation of Cl and O_2 respectively. The decomposition of ClOO on the subnanosecond timescale was later confirmed by FPP work [98].

Although it has been shown that ClOO is produced following OClO photolysis, the mechanism by which this isomer is formed remained unclear. Two mechanisms for ClOO formation have been proposed: OClO photoisomerization and geminate recombination of the primary photofragments. Photochemical studies of gaseous

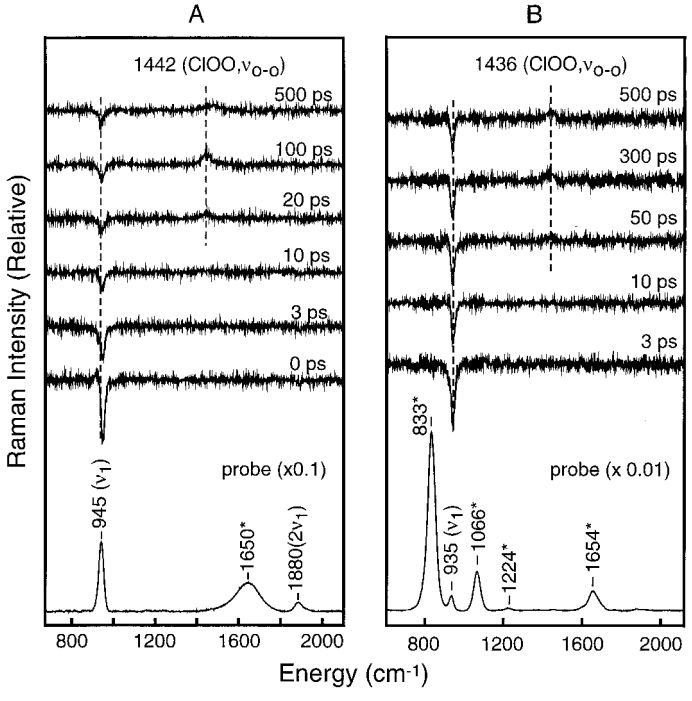

Figure 10. Time-resolved resonance Raman Stokes difference spectra of OClO dissolved in (*a*) water and (*b*) fluorotrichloromethane. Data were obtained using a 390 nm and 260 nm pump and probe beams respectively. The temporal delay between the pump and the probe at which a given spectrum was obtained is indicated. The probe-only spectrum is presented at the bottom of each panel. Transitions marked with an asterisk in the probe-only spectra are due to the solvent.

OClO by Vaida and coworkers invoked ClOO production via photoisomerization to explain resonances observed in the resonance-enhanced multiphoton photoionization spectra of Cl produced following OClO photoexcitation [9, 26]. Solution-phase studies have also been largely interpreted in terms of the photoisomerization model [38, 80, 98]. In contrast, studies in low-temperature matrixes and on ice surfaces have used both the photoisomerization and the geminate recombination models to explain ClOO production in these environments [32, 33, 36, 101, 103]. Finally, theoretical studies of OClO and ClOO by Gole provided a plausible mechanism for OClO photoisomerization [104]; however, later computational studies by Peterson and Werner were not supportive of this model [55–57].

To study the mechanism of ClOO formation, we have extended our two-colour TRRR studies to OClO dissolved in trichlorofluoromethane (Freon-11) [45]. This solvent was chosen since it is an aprotic solvent in which the absence of solvent hydrogen bonding is expected to produce a solvent cage that is more labile to escape of the primary photoproducts. Greater cage escape should result in a reduction in ClOO production if this species is produced by photofragment recombination. As described earlier, a similar motivation led us to perform TRRR studies in acetonitrile [82]; however, this solvent could not be employed here because of spectral overlap with ClOO. In this study, the geminate-recombination quantum yield in Freon-11 was determined first by monitoring the evolution in optical density at 390 nm

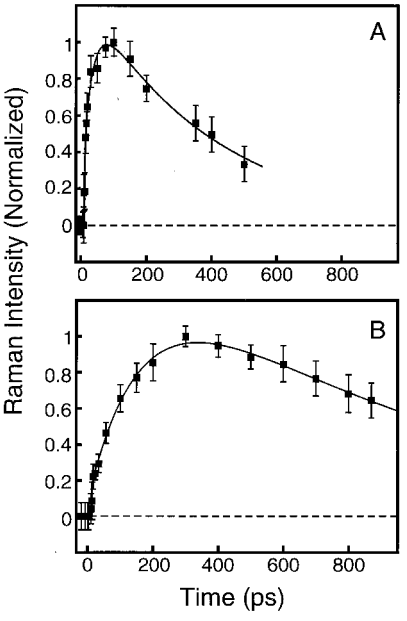

Figure 11. (*a*) Intensity of the ClOO transition at 1442 cm^{-1} in water as a function of time delay. The data were fitted by a sum of two exponentials convolved with the instrument response resulting in appearance and decay time constants of 27.9 ± 4.5 ps and 398 ± 50 ps respectively. In addition, inclusion of a 12.7 ± 1.5 ps dwell relative to zero time was necessary to reproduce the data. (*b*) Intensity of the same ClOO transition in Freon-11 as a function of time delay. The data were fitted by a sum of two exponentials convolved with the instrument response resulting in appearance and decay time constants of 172 ± 30 ps and 864 ± 200 ps respectively. In addition, inclusion of a 13 ± 0.4 ps dwell relative to zero time was necessary to reproduce the data.

following OClO photoexcitation. OClO dominates the optical-density evolution at this probe wavelength; therefore, these data provided a measure of photoinitiated ground-state OClO depletion and subsequent recovery via geminate recombination. These studies demonstrated that the geminate recombination quantum yield is only 0.3 ± 0.1 in Freon-11, substantially reduced relative to water and consistent with the expectation outlined above.

TRRR Stokes difference spectra of OClO in Freon-11 are presented in figure 10(*b*). Similar to the behaviour observed in water, negative intensity for OClO transitions is observed corresponding to ground state depletion by photolysis. The depletion in OClO intensity evident at later delays is significantly greater than in water, consistent with a reduction in the geminate-recombination quantum yield. The presence of positive intensity at 1436 cm^{-1} demonstrates that ClOO is also produced in Freon-11; however, the appearance of this species occurs on a significantly slower timescale relative to water. Figure 11(*b*) presents the temporal evolution in the scattering intensity for the 1436 cm^{-1} transition in Freon-11. The data were best fitted by a sum of two exponentials convolved with the instrument response resulting in appearance and decay time constants of 172 ± 30 ps and 864 ± 200 ps respectively. Experiments were performed in which the relative ClOO production quantum yields in water and Freon-11 were determined [45]. The ClOO

maximum scattered intensities were found to be equivalent in Freon-11 and water within experimental error (±20%). Given the differences in production and decay time constants, equivalent intensity does not necessarily mean that the ClOO production quantum yield is solvent independent. However, a check of the expected ClOO concentration profiles employing the time constants determined above in conjunction with a sequential reaction mechanism demonstrates that similar ClOO intensities are indeed expected at 100 and 300 ps delay in water and Freon-11 respectively if the ClOO quantum yield is independent of solvent. Therefore, the similarity in maximum ClOO scattering intensity demonstrates that the quantum yield of ClOO production is similar between these two solvents. The solvent independence of the ClOO production quantum yield combined with a 3-fold reduction in geminate-recombination efficiency in Freon-11 suggests that ground-state ClOO is not produced by primary-photoproduct recombination. The importance of geminate recombination was questionable from a kinetic standpoint since the ClOO appearance time constant is 2 orders of magnitude greater than the subpicosecond time constant for recombination resulting in ground-state OClO production. Therefore, the results obtained from this TRRR study can be viewed as supportive of the photoisomerization model.

The results presented above provide insight into the mechanism of Cl production following OClO photoexcitation. FPP studies have shown that, in water, Cl formation is a bifurcated process where the majority (80%) of Cl is formed with a time constant of ~6 ps while the remainder (20%) is formed on the ~100 ps timescale [98]. The later-time production of Cl arises from the ground-state decomposition of ClOO. Therefore, the question remains as to the mechanism for fast or 'prompt' Cl production. This photoproduct channel has been assigned to direct dissociation of OClO via the bending coordinate [16, 17, 56]. However, 6 ps is rather slow for direct dissociation, and recent studies suggest that internal conversion of the optically prepared excited state occurs in ~200 fs in aqueous solution [71]. Therefore, we have proposed an alternative mechanism for Cl production. As discussed above, a fraction of photoexcited OClO undergoes photoisomerization on the $^2B_2$ surface to produce ClOO in an excited $^2A'$ state. We propose that the majority of ClOO continues along the reaction coordinate and forms a distorted intermediate resembling the Cl and O_2 photofragments and that this intermediate undergoes dissociation into Cl and O_2 with a time constant of 6 ps. The remainder of excited-state ClOO undergoes internal conversion to the $^2A''$ ground state and subsequent decomposition into Cl and O_2. Evaluation of this model is entirely dependent on ascertaining the nature of the lower-energy excited states of ClOO, since *ab initio* studies predict that all ClOO excited states are dissociative [79]. However, similar calculations in the condensed phase have not been performed. In the presence of solvent, these surfaces might be modified to allow for the formation of a stable, excited-state ClOO. In support for this hypothesis, recent *ab initio* work has shown that asymmetric distortions of the $^2B_2$ surface that lead to symmetry breaking (C_{2v} to C_s) favour an increase in the well depth of the $^2A'$ state of ClOO [56].

4. Current picture of aqueous OClO photochemistry

The TRRR studies outlined here have provided insight into the condensed-phase photochemistry of OClO. As discussed in the introduction, $\Phi_{Cl} = 0.1$ such that the

dominant photochemical channel in solution is ClO and O production. These photoproducts undergo geminate recombination on the subpicosecond timescale resulting in the reformation of ground-state OClO. Once formed, OClO undergoes vibrational relaxation with a rate that is solvent dependent. Recent theoretical work has shown this solvent dependence largely arises from changes in the solvent force spectrum accompanying a change in solvent. The remainder of photoexcited OClO goes on to produce Cl through a bifurcated process. ClOO production and decay represents the minor Cl production channel, accounting for only 20% of Cl production. The remainder of Cl is produced by a 'direct' process, the details of which are not well understood. Transient absorption studies have shown that this process involves an intermediate that decomposes to form Cl with a time constant of ~6 ps; however, the identity of this intermediate has yet to be established.

Although much progress has been made in understanding the environment-dependent reaction dynamics of OClO, there are many unresolved questions that are currently being addressed. First, identification of the intermediate species responsible for the majority of Cl production is the primary issue in OClO photochemistry. Second, gas-phase studies have shown that the Cl production quantum yield is dependent on actinic wavelength [17], and it is currently unclear whether similar behaviour occurs in condensed environments. Recent FPP studies of aqueous OClO have presented intriguing evidence that the excited-state dynamics is dependent on the initial vibronic level produced [96]. This result strongly suggests that a change in the actinic wavelength will have a pronounced effect on photoproduct formation. However, photochemical action spectra of OClO isolated in clusters suggest that the Cl production quantum yield is not dependent on actinic wavelength [29]. Therefore, the variation in OClO photochemistry with actinic wavelength remains an important, yet unanswered, question. Third, the TRRR studies presented were interpreted in terms of ClOO production via OClO photoisomerization. It is unclear whether this behaviour is unique to OClO or whether photoisomerization is a general feature of halooxide photochemistry. Recent work in our laboratory has found that the photoisomerization of ClOCl to form ClClO occurs on the tens of picoseconds timescale, similar to the timescale for ClOO production, suggesting that this may be a general feature of halooxide photochemistry in condensed environments [105]. Finally, the work outlined here was performed with an eye towards the chemistry of halooxides at the condensed phase–air interface. Issues such as solute orientation, the efficiency of geminate recombination and the quantum yield for Cl production in such environments are important issues that remain unexplored. The extension of this work to the interfacial domain will be a challenging and important avenue of study.

Acknowledgments

We would like to acknowledge the contributions of our coworkers Bethany Barham, Anthony Esposito, Catherine Foster, Steven Mayer, Ryan McLaughlin, Matthew Philpott and Carsten Thomsen (Aarhus University, Denmark). The National Science Foundation is acknowledged for their support of this work (CHE-9701717 and CHE-0091320). Acknowledgment is also made to the donors of the Petroleum Research Fund, administered by the American Chemical Society. P.J.R. is an Alfred P. Sloan Fellow, and is a Cottrell Scholar of the Research Corporation.

References

[1] Farman, J. C., Gardiner, B. G., and Shanklin, J. D., 1985, *Nature*, **315**, 207.
[2] Rowland, F. S., 1991, *Annu. Rev. phys. Chem.*, **42**, 731.
[3] Sander, S. P., Friedl, R. R., and Francisco, J. S., 1995, in *Progress and Problems in Atmospheric Chemistry*, edited by J. R. Barker (Singapore: World Scientific).
[4] Molina, M. J., Molina, L. T., and Golden, D. M., 1996, *J. phys. Chem.*, **100**, 12888.
[5] Wayne, R. P., 1991, *The Chemistry of Atmospheres* (Oxford: Oxford Science).
[6] Finlayson-Pitts, B. J., and Pitts, J. N., Jr., 2000, *Chemistry of the Upper and Lower Atmosphere* (San Diego, CA: Academic Press).
[7] Solomon, S., Garcia, R. R., Rowland, F. S., and Wuebbles, D. J., 1986, *Nature*, **321**, 755.
[8] Solomon, S., Borrmann, S., Garcia, R. R., Portmann, R., Thomason, L., Poole, L. R., Winker, D., and McCormick, M. P., 1997, *J. geophys. Res.*, **102**, 21411.
[9] Vaida, V., Solomon, S., Richard, E. C., Ruhl, E., and Jefferson, A., 1989, *Nature*, **342**, 405.
[10] Vaida, V., Goudjil, K., Simon, J. D., and Flanders, B. N., 1994, *J. mol. Struct.*, **61**, 133.
[11] Vaida, V., and Simon, J. D., 1995, *Science*, **268**, 1443.
[12] Reid, P. J., 2001, *Acc. chem. Res.*, **34**, 69.
[13] Sessler. J., Chipperfield, M. P., Pyle, J. A., and Toumi, R., 1995, *Geophys. Res. Lett.*, **22**, 687.
[14] Miller, H. L., Sanders, R. W., and Solomon, S., 1999, *J. geophys. Res.*, **104**, 18769.
[15] Wagner, T., Carsten, L., Pfeilsticker, K., and Platt, U., 2001, *J. geophys. Res*, **106**, 4971.
[16] Davis, H. F., and Lee, Y. T., 1992, *J. phys. Chem.*, **96**, 5681.
[17] Davis, H. F., and Lee, Y. T., 1996, *J. chem. Phys.*, **105**, 8142.
[18] Bishenden, E., Haddock, J., and Donaldson, D. J., 1991, *J. phys. Chem.*, **95**, 2113.
[19] Bishenden, E., and Donaldson, D. J., 1993, *J. chem. Phys.*, **99**, 3129.
[20] Bishenden, E., and Donaldson, D. J., 1994, *J. chem. Phys.*, **101**, 9565.
[21] Baumert, T., Herek, J. L., and Zewail, A. H., 1993, *J. chem. Phys.*, **99**, 4430.
[22] Delmdahl, R. F., Bakker, D. L. G., and Parker, D. H., 2000, *J. chem. Phys.*, **112**, 5298.
[23] Delmdahl, R. F., Ullrich, S., and Gericke, K.-H., 1998, *J. phys. Chem.* A, **102**, 7680.
[24] Delmdahl, R. F., Baumfartel, S., and Gericke, K.-H., 1996, *J. chem. Phys.*, **194**, 2883.
[25] Roth, M., Maul, C., and Gericke, K.-H., 1997, *J. chem. Phys.*, **107**, 10582.
[26] Ruhl, E., Jefferson, A., and Vaida, V., 1990, *J. phys. Chem.*, **94**, 2990.
[27] Flesch, R., Wassermann , B., Rothmund, B., and Ruhl, E., 1994, *J. phys. Chem.*, **98**, 6263.
[28] Lawrence, W. G., Clemitshaw, K. C., and Apkarian, V. A., 1990, *J. geophys. Res.*, **95**, 18591.
[29] Kreher, C. J., Carter, R. T., and Huber, J. R., 1999, *J. chem. Phys.*, **110**, 3309.
[30] Kreher, C. J., Carter, R. T., and Huber, J. R., 1998, *Chem. Phys. Lett.*, **286**, 389.
[31] Furlan, A., Scheld, H. A., and Huber, J. R., 1997, *J. chem. Phys.*, **106**, 6538.
[32] Arkell, A., and Schwager, I., 1967, *J. Am. Chem. Soc.*, **89**, 5999.
[33] Mueller, H. S. P., and Willner, H., 1993, *J. phys. Chem.*, **97**, 10589.
[34] Lanzendorf, E. J., and Kummel, A. C., 1996, *Geophys. Res. Lett.*, **23**, 1251.
[35] Adrian, F. J., Bohandy, J., and Kim, B. F., 1986, *J. chem. Phys.*, **85**, 2692.
[36] Pursell, C. J., Conyers, J., Alapat, P., and Parveen, R., 1995, *J. phys. Chem.*, **99**, 10433.
[37] Dunn, R. C., and Simon, J. D., 1992, *J. Am. Chem. Soc.*, **114**, 4856.
[38] Dunn, R. C., Flanders, B. N., and Simon, J. D., 1995, *J. phys. Chem.*, **99**, 7360.
[39] Thøgersen, J., Thomsen, C. L., Poulsen, J., and Keiding, S. R., 1998, *J. phys. Chem.* A, **102**, 4186.
[40] Poulsen, J. A., Thomsen, C. L., Keiding, S. R., and Thøgersen, J., 1998, *J. chem. Phys.*, **108**, 8461.

[41] THØGERSEN, J., JEPSEN, P. U., THOMSEN, C. L., POULSEN, J., BYBERG, J. R., and KEIDING, S. R., 1997, *J. phys. Chem.*, **101**, 3317.
[42] PHILPHOTT, M. J., CHARALAMBOUS, S., and REID, P. J., 1997, *Chem. Phys. Lett.*, **281**, 1.
[43] BURSA, M. A., PERISSINOTTI, L. J., CHURIO, M. S., and COLUSSI, A. J., 1996, *J. Photochem. Photobiol.* A., **101**, 105.
[44] THOMSON, C. L., PHILPHOT, M. P., HAYES, S. C., and REID, P. J., 2000, *J. chem. Phys.*, **112**, 505.
[45] HAYES, S. C., THOMSEN, C. L., and REID, P. J., 2001, *J. chem. Phys.*, **115**, 11228.
[46] GRAHAM, J. D., Roberts, J. T., Brown, L. A., and VAIDA, V., 1996, *J. phys. Chem.*, **100**, 3115.
[47] BROWN, L. A., VAIDA, V., HANSON, D. R., GRAHAM, J. D., and ROBERTS, J. T., 1996, *J. phys. Chem.*, **100**, 3121.
[48] COON, J. B., 1940, *Phys. Rev.*, **58**, 926.
[49] COON, J. B., 1946, *J. chem. Phys.*, **14**, 665.
[50] MULLIKEN, R. A., 1958, *Can. J. Chem.*, **36**, 10.
[51] LAWLESS, M. K., REID, P. J., and MATHIES, R. A., 1994, in *Ultrafast Dynamics of Chemical Systems*, edited by J. D. Simon (Amsterdam: Klower), pp. 267–287.
[52] RICHARD, E. C., and VAIDA, V., 1991, *J. chem. Phys.*, **94**, 153.
[53] RICHARD, E. C., and VAIDA, V., 1991, *J. chem. Phys.*, **94**, 163.
[54] BRAND, J. C. D., REDDING, R. W., and RICHARDSON, A. W., 1970, *J. mol. Spectrosc.*, **34**, 399.
[55] PETERSON, K. A., and WERNER, H.-J., 1992, *J. chem. Phys.*, **96**, 8948.
[56] PETERSON, K. A., and WERNER, H.-J., 1996, *J. chem. Phys.*, **105**, 9823.
[57] PETERSON, K. A., 1998, *J. chem. Phys.*, **109**, 8864.
[58] XIE, D., and GUO, H., 1999, *Chem. Phys. Lett.*, **307**, 109.
[59] ESPOSITO, A., FOSTER, C., BECKMAN, R., and REID, P. J., 1997, *J. phys. Chem.* A, **101**, 5309.
[60] REID, P. J., ESPOSITO, A. P., FOSTER, C. E., and BECKMAN, R. A., 1997, *J. chem. Phys.*, **107**, 8262.
[61] FOSTER, C. E., and REID, P. J., 1998, *J. phys. Chem.* A, **102**, 3541.
[62] ESPOSITO, A. P., STEDL, R., JONSSON, H., REID, P. J., and PETERSON, K. A., 1999, *J. phys. Chem.* A, **103**, 1748.
[63] FOSTER, C. E., BARHAM, B. P., and REID, P. J., 2001, *J. chem. Phys.*, **114**, 4892.
[64] MYERS, A. B., and MATHIES, R. A., 1987, in *Biological Applications of Raman Spectroscopy*, Vol. 2, *Resonance Raman Spectra of Polyenes and Aromatics*, edited by T. G. Spiro (New York: Wiley), pp. 1–58.
[65] MYERS, A. B., 1994, *Chem. Phys.*, **180**, 215.
[66] MYERS, A. B., 1997, *J. Raman Spectrosc.*, **28**, 389.
[67] LEE, S.-Y., and HELLER, E. J., 1979, *J. chem. Phys.*, **71**, 4777.
[68] TANNOR, D. J., and HELLER, E. J., 1982, *J. chem. Phys.*, **77**, 202.
[69] MYERS, A. B., 1998, *Annu. Rev. phys. Chem.*, **49**, 267.
[70] DUNN, R. C., ANDERSON, J. L., FOOTE, C. S., and SIMON, J. D., 1993, *J. Am. Chem. Soc.*, **115**, 5307.
[71] HAYES, S. C., COOKSEY, C. C., WALLACE, P. M., and REID, P. J., 2001, *J. phys. Chem.* A, **105**, 9819.
[72] BERG, M. A., 1994, *Chem. Phys. Lett.*, **228**, 317.
[73] BERG, M. A., 1998, *J. phys. Chem.* A, **102**, 17.
[74] BERG, M. A., 1999, *J. chem. Phys.*, **110**, 8577.
[75] MUKAMEL, S., 1985, *J. chem. Phys.*, **82**, 5398.
[76] AHERNE, D., TRAN, V., and SCHWARTZ, B. J., 2000, *J. phys. Chem.* B, **104**, 5382.
[77] LADANYI, B. M., and STRATT, R. M., 1995, *J. phys. Chem.*, **99**, 2502.
[78] DUNN, R. C., RICHARD, E. C., VAIDA, V., and SIMON, J. D., 1991, *J. phys. Chem.*, **95**, 6060.
[79] JAFRI, J. A., LENGSFIELD III, B. H., and PHILLIPS, D. H., 1985, *J. chem. Phys.*, **83**, 1693.
[80] CHANG, Y. J., and SIMON, J. D., 1996, *J. phys. Chem.*, **100**, 6406.
[81] HAYES, S. C., PHILPOTT, M. J., and REID, P. J., 1998, *J. chem. Phys.*, **109**, 2596.

[82] HAYES, S. C., PHILPOTT, M. P., MAYER, S. G., and REID, P. J., 1999, *J. phys. Chem.* A, **103**, 5534.
[83] PHILPOTT, M. J., HAYES, S. C., THOMSEN, C. L., and REID, P. J., 2001, *Chem. Phys.*, **263**, 389.
[84] SCHWARTZ, B. J., KING, J. C., and HARRIS, C. B., 1994, in *Ultrafast Dynamics of Chemical Systems*, edited by J. D. Simon (Dordrecht: Kluwer).
[85] WALHOUT, P. K., ALFANO, J. C., THAKUR, K. A. M., and BARBARA, P. F., 1995, *J. phys. Chem.*, **99**, 7568.
[86] KIVINEN, A., and MURTO, J., 1967, *Suom. Kemistil.*, **40**, 6.
[87] KRUEGER, P. J., and METTEE, H. D., 1964, *Can. J. Chem.*, **42**, 340.
[88] BLAINEY, P. C., and REID, P. J., 2001, *Spectrochim. Acta* A, **57**, 2763.
[89] HARRIS, A. L., BROWN, J. K., and HARRIS, C. B., 1988, *Annu. Rev. phys. Chem.*, **39**, 341.
[90] HAMM, P., LIM, M., and HOCHSTRASSER, R. M., 1997, *J. chem. Phys.*, **107**, 10523.
[91] LU, Z.-M., and KELLMAN, M. E., 1997, *J. chem. Phys.*, **107**, 1.
[92] LI, Z., XIAO, L., and KELLMAN, M. E., 1990, *J. chem. Phys.*, **92**, 2251.
[93] GOMEZ LLORENTE, J. M., HAHN, O., and TAYLOR, H., 1990, *J. chem. Phys.*, **92**, 2762.
[94] POULSEN, J., NYMAND, T. M., and KEIDING, S. R., 2001, *Chem. Phys. Lett.*, **343**, 581.
[95] CHORNY, I., VIECELI, J., and BENJAMIN, I., 2002, *J. chem. Phys.*, **116**, 8904.
[96] FIDDER, H., TSCHIRSCHWITZ, F., DUHR, O., and NIBBERING, E. T. J., 2001, *J. chem. Phys.*, **114**, 6781.
[97] THOMSEN, C. L., PHILPOTT, M. P., HAYES, S. C., and REID, P. J., 2000, *J. chem. Phys.*, **112**, 505.
[98] THOMSEN, C. L., REID, P. J., and KEIDING, S. R., 2000, *J. Am. Chem. Soc.*, **122**, 12795.
[99] MAULDIN III, R. L., BURKHOLDER, J. B., and RAVISHANKARA, A. R., 1992, *J. phys. Chem.*, **96**, 2582.
[100] MORRIS, E. D., and JOHNSTON, H. S., 1968, *J. Am. Chem. Soc.*, **90**, 1918.
[101] JOHNSSON, K., ENGDAHL, A., OUIS, P., and NELANDER, B., 1992, *J. phys. Chem.*, **96**, 5778.
[102] JOHNSSON, K., ENGDAHL, A., OUIS, P., and NELANDER, B., 1993. *J. mol. Struct.*, **293**, 137.
[103] GANE, M. P., WILLIAMS, N. A., and SODEAU, J. R., 1997, *J. Chem. Soc., Faraday Trans.*, **93**, 2747.
[104] GOLE, J. L., 1980, *J. phys. Chem.*, **84**, 1333.
[105] COOKSEY, C. C., and REID, P. J., in preparation.